Decomposition-Based Assembly Synthesis Based on Structural Considerations

F. A. Yetis
Graduate Student Research Assistant

K. Saitou
Assistant Professor

Department of Mechanical Engineering,
University of Michigan,
Ann Arbor, MI 48109

This paper presents a method for decomposition of structural products in order to provide the product designer with choices for feasible assemblies. The synthesis of assemblies is done by decomposing a complex structure obtained via structural topology optimization into an assembly of multiple structural members with simpler geometries. The aim is at providing a systematic approach to explore a large number of decompositions prior to the detailed component design phase. Initially, the structure, which is represented as a bitmap image, is transformed to a graph with equivalent topology through application of image processing algorithms. Then, the obtained graph is decomposed by a genetic algorithm into subgraphs using stiffness-based criteria. Results for an example structure are given to clarify and discuss the method. [DOI: 10.1115/1.1519276]

1 Introduction

Most structural products, from a simple chair frame to an automobile body, are manufactured through assembly of various components which have simpler geometries than the end product. Assembly synthesis is the decision of which components to assemble together to achieve the end product and is done by decomposition of the end product design prior to the detailed component design phase. From a structural point of view, it is not desirable to introduce joints into the structure since they will decrease the strength of the product. However, most designs are impossible to manufacture as one single component. Therefore, assembly synthesis is an inevitable step in most design cases.

Figure 1 shows an example of the decomposition of an automotive body front consisting of the external panels (hood and outer fenders) and the internal structures (inner fenders and radiator support) that connect to the rest of the internal body frame. In industry, such decompositions are typically done prior to the detailed design of individual components, taking into account functionality, manufacturability or geometry issues. However, the process is nonsystematic and can result in the decompositions that might overlook one or more of the following criteria that cause problems in the detailed design phases:

- **Structural strength:** The joints introduced to the structure due to decomposition decrease the strength of the initial design. This effect has to be kept to a minimum.
- **Manufacturability and assembleability:** The decomposition should result in components and joint features/methods which are physically and economically feasible.

By observing these criteria during the assembly synthesis, problems in subsequent design phases can be substantially reduced. The method presented in this paper aims at achieving a systematic decomposition process applicable during conceptual design stages, with major emphasis on structural characteristics and minor emphasis on assembleability. Other criteria will be included in future work. The presented approach intends to provide the designer with feedback about possible decompositions prior to the detailed design phase. By applying the presented method prior to the detailed design phase, changes in detailed design due to structural and other issues are minimized which may be costly and time consuming.

In our method, a structure obtained via structural topology optimization is decomposed into an assembly consisting of multiple structural members with simpler geometries. There are two main steps in the process developed:

1. A two-dimensional bitmap image of a structure obtained via structural topology optimization is transformed to a product topology graph through application of image processing algorithms.
2. The product topology graph is decomposed into subgraphs by using a genetic algorithm which results in a decomposition of the product with chosen mating features.

Finally, results for an example structure are presented to demonstrate the method and to discuss the results.

2 Related Work

Design for assembly (DFA) is a class of design methodologies for improving product design based on assembly considerations to realize easy and low-cost assembly [1]. Based on the results from the seminal work on assembly modeling and sequence generation [2–5] a number of researchers attempted the integration of assembly planning and DFA [6–8]. Although proven effective, these approaches require detailed component geometry as input, hence limiting their application to early phases of the design process.

To overcome this limitation, Mantripragada et al. [9,10] developed a method to predict the propagation of dimensional variations based on Datum Flow Chain, a logical relationship among the component dimensions. Although this approach does not require detailed component geometry, the product decomposition must be specified a priori by a designer.

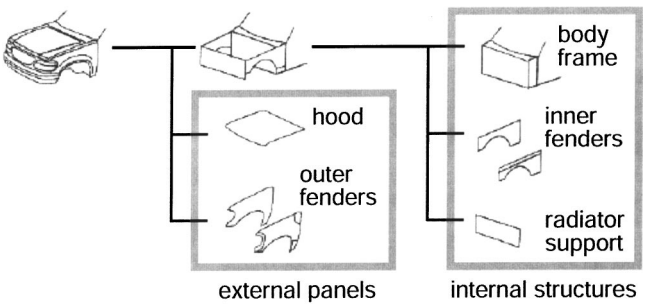

Fig. 1 Example of decomposition of an automobile body front

Contributed by the Design Theory and Methodology Committee for publication in the JOURNAL OF MECHANICAL DESIGN. Manuscript received February 2000; revised March 2001. Associate Editor: J. Cagan.

Graph decomposition [11] has been applied to mechanical design, such as model-based decomposition of design problems [12] and manufacturing feature recognition [13]. Among the most relevant is the application to automatic assembly sequence generation, where a disassembly sequence (assumed to be the reverse of an assembly sequence) is generated by sequential binary decompositions (*i.e.*, cuts) of a graph of connections of an assembled product [2–5]. Feasibility of each binary decomposition is determined by checking the precedence relationship of two subassemblies subject to partition using human input [2–3] or geometric reasoning [5].

Recently, Wang et al. [14,15] developed a system which decomposes an unfolded sheet metal product based on the decomposition of a spanning tree of the face-adjacency graph of the product. Although their focus is similar to the presented research, the system does not consider the structural issues of the product. Also, the approach does not address the issue of dimensional errors in cutting, bending and joining.

3 Assembly Synthesis Method

The proposed assembly synthesis method [16–18] consists of two major procedures. First, the topology graph of a structure, which is obtained via structural topology optimization, is constructed by application of image processing algorithms on the two-dimensional bitmap image of the structure. The next step is the decomposition of the topology graph using a genetic algorithm. It should be noted that the focus (also an original contribution) of the current work is the *extraction and decomposition* of the structural topology, rather than the generation of the optimal structural topology that have been addressed previously by a number of researchers.

3.1 Structural Topology Optimization. Structural topology design methods, such as the homogenization design method [19] and the genetic algorithm based [20], enable top-down synthesis of an optimal structure topology that fits within a specified design domain from the specification of loading and boundary conditions. As illustrated in Fig. 2, these methods take as input the design domains and the loading and boundary conditions, and then produce through finite element analyses a discretized image (bitmap or grayscale) of an optimal material distribution in the design domain which, for example, maximizes stiffness at the loading point subject to weight constraints. In most cases, each pixel in the output image corresponds to a finite element. The methods also allow the design domain to be multiply-connected (*i.e.*, to have holes).

3.2 Construction of Product Topology Graphs. Figure 3 outlines the flow of the transformation process. First, topology of the output image is extracted by identifying the distinct segments in the output image (Fig. 3(*b*)). Next, the resulting segments are labeled, and their connectivities are checked to produce a product topology graph (Fig. 3(*c*)). The extraction of product topology is accomplished by the successive application of standard digital image processing algorithms such as dilation, skeletonization, and the Hough transform [21], as well as nonstandard algorithms such as primary line extraction and topological segmentation.

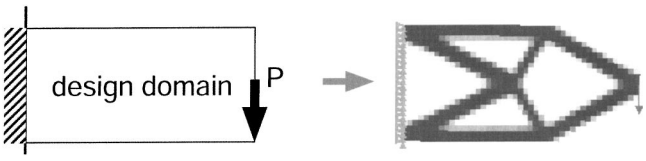

Fig. 2 Structural topology design method: The right figure shows a structure with maximum stiffness occupying 40% of the design domain. The result is obtained by using Topology Optimization Web site at the Technical University of Denmark (http://www.topopt.dtu.dk/).

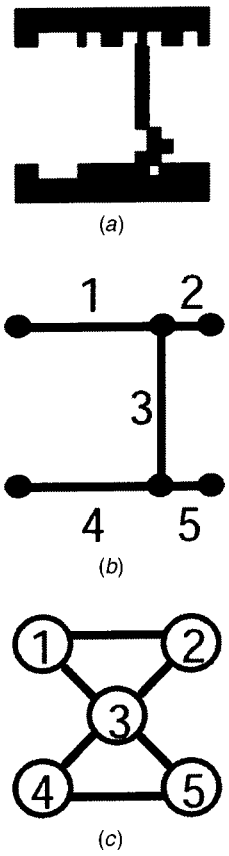

Fig. 3 Transformation of a structural topology optimization output to a product topology graph. (*a*) output image, (*b*) extraction of product topology, and (*c*) resulting product topology graph. The I-beam like image was adopted from [20].

Figure 4 illustrates a sequence of these image transformations applied to an example I-beam like image [20] using the preliminary implementation of the transformation algorithms. A brief description of each step is given in the following. Although the description assumes a bitmap image as an input, it can be easily generalized to a gray scale image with a prior application of an appropriate thresholding method.

3.2.1 Dilation. It fattens the image by filling small, isolated holes and expanding the image boundary (Fig. 4(*b*)). It scans the image and turns a pixel on if a majority of the neighboring pixels are also on. Definition of majority and neighbor determines the effects of fattening. Since dilation is to eliminate small voids or nonsmooth edges prior to skeletonization, it is unnecessary for smooth images such as the structure in Fig. 2.

3.2.2 Skeletonization. It has an opposite effect to dilation. It thins the image by expanding small, isolated holes and shrinking the image boundary (Fig. 4(*c*)). It scans the image and turn off a pixel if a majority of the neighboring pixels are also off. Definition of majority and neighbor determines the effects of thinning. Applying dilation before skeletonization prevents the resulting skeleton from being affected by noises in the original image.

3.2.3 Hough Transform. Although obvious to human eyes, bitmap does not contain information on distinguishable ''lines'' in the image necessary for the subsequent decomposition process. For this, Hough transform [21] a standard technique for feature extraction of digital images, is applied after skeletonization. It detects lines in a bitmap image by mapping the image in the x-y space to a parameter space (the θ-ρ space) using the normal representation of a line in x-y space:

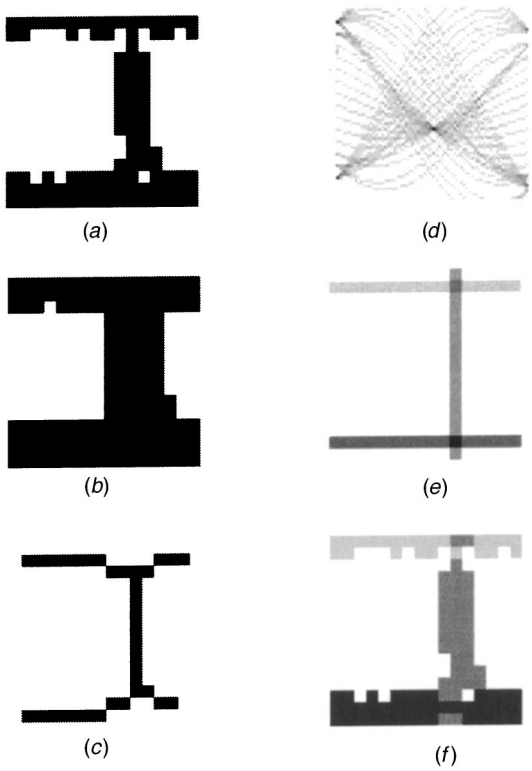

Fig. 4 An example of product topology extraction: (*a*) original image, (*b*) dilation, (*c*) skeletonization, (*d*) initial Hough transform (shown in θ-ρ space), (*e*) primary line extraction, and (*f*) topological segmentation.

$$x \cos \theta + y \sin \theta = \rho \tag{1}$$

Since a pixel (x_i, y_i) *x-y* space corresponds to a sinusoidal curve $x_i \cos \theta + y_i \cos \theta = \rho$ in the θ-ρ space, collinear pixels in the *x-y* space have the intersecting sinusoidal lines in the θ-ρ space. Conversely, an intersection point (θ_n, ρ_n) in the θ-ρ space corresponds to a line in the *x-y* space. Therefore, all lines passing through arbitrary pairs of pixels in the image are found by checking the intersection points in the θ-ρ space. The discretization of the θ-ρ space to compute the sinusoidal lines determines the accuracy of the detected lines.

The Hough transform is repeatedly applied in the primary line extraction algorithm described below. Figure 4(*d*) shows the θ-ρ space from the initial application to the skeletonized image. A generalized form of the Hough transform uses a spline representation of a curve to detect arbitrary curves in the image [22], which will be incorporated in the future implementation.

3.2.4 Primary Line Extraction. This algorithm abstracts the topology of the skeletonized image by selecting primary lines in the *x-y* space based on the number of pixels they pass through. Basic procedure is as follows.

1. Do the Hough transform of the image.
2. Select an intersection point in the θ-ρ space with the maximum number of intersecting lines. If the maximum number is below a prespecified value, return.
3. Remove pixels in the image corresponding to the intersecting lines in 2 and goto 1.

Figure 4(*e*) shows the extracted three primary lines shown in a different gray scale. The prespecified value in the step 2 to cut off the iteration determines the ''level of abstraction'' of the extracted topology. The repeated application of the Hough transform is needed since the pixels removed in step 3 may also have been on the lines not selected in step 2. However, it does not generally add a significant computational overhead since the number of unremoved pixels rapidly decreases after a few iterations. After the above steps, all intersections among the extracted primary lines are also calculated, and the segments of the intersecting primary lines are labeled separately.

3.2.5 Topological Segmentation. It associates each pixel in the original image to each segment of the primary lines identified above. For each pixel in the original image, it calculates the distances to all segments of primal lines, and associates the pixel with the primal line segment with the minimum distance. If a pixel is approximately equidistance to multiple segments, it corresponds to an intersection of the primary lines. Figure 4(*f*) shows the original image shaded with three distinct segments corresponding to the three primal lines in Fig. 4(*e*).

Occasionally, however, the topological segmentation yields a segmented image with stand-alone (disconnected) pixels at the intersection of multiple segments. In such cases, the following postprocessing is necessary to re-assign these pixels to another primal line so they can be connected.

1. Select a segment in an image obtained by the topological segmentation. If all segments have been checked, return.
2. Count the number of disconnected sub-segments. If the number is one, go to 1. Otherwise let the largest subsegment be the primal segment.
3. For each pixel not belonging to the primal segment, reassign the pixel to the primal line to which the majority of the surrounding pixels belong.
4. Go to 1.

After the completion of the extraction of product topology, a product topology graph can be easily constructed by labeling each segment of the primary lines and each intersection among the primary lines, with a node and an edge in a graph data structure, respectively.

3.3 Decomposition of Product Topology Graphs. We are interested in obtaining the decomposition of a given structure to the desired number of components that minimally reduces the structural strength due to the introduction of joints. This is achieved by decomposing the product topology graph and the corresponding product geometry as illustrated in Fig. 5. The following assumptions are made at this stage:

- Joining method at every joint is spot weld; hence joints are strong for shear and compressive loading, but weak in tensile loading.
- The only joint feature considered is the weld angle which is chosen from discrete set of possible values.
- Number of components desired is specified by designer.
- The structure can be decomposed only at the location corresponding to the edges of the topology graph.

Even for a small number of possible joint locations and weld angles, the number of potential decompositions to be considered will be very large due to the combinatorial nature of the underlying graph decomposition problem. In this paper, therefore, the problems is treated as an optimization problem and solved using a genetic algorithm (GA). Posing the problem as an optimization allows the efficient exploration of multiple high-performance decompositions based on given criteria, depending on the weight factor of each criterion. The following sections formulate the mathematical model of the optimization problem and describe the method used to solve it which is GA.

3.4 Mathematical Model

3.4.1 Definition of the Design Variables. The optimal decomposition can be posed as a graph partitioning problem [11]. The members of the structure are mapped to nodes and the intersections are mapped to multiple edges since they can be joining

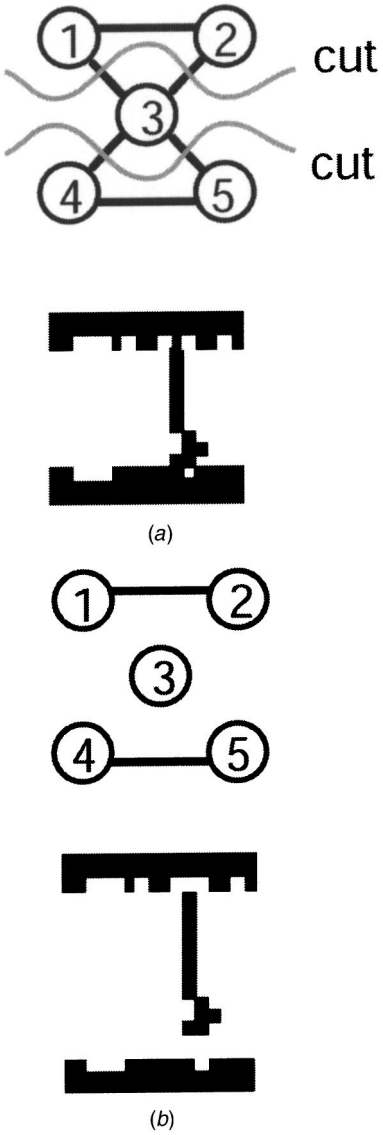

Fig. 5 Decomposition of a product topology graph and the corresponding product geometry (*a*) before decomposition and (*b*) after decomposition

more than two members. Therefore, the whole structure can be represented as a graph $G=(V,E)$ with node set V and edge set E. The problem of optimal decomposition becomes one of finding a partition, P, of the node set V such that the objective function, $c(P)$, is maximized.

Note that the number of nonempty subsets, k, of V, which constitute the optimal partition, is not defined. Mating features at the joints are major factors affecting structural strength therefore a set, F, of mating features must also be defined to be able to evaluate different decompositions. As based on previously stated assumptions, F is the set of possible mating angles at the welded joints, *i.e.*, the only mating feature considered is the weld angle.

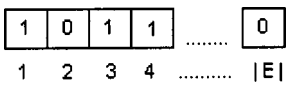

Fig. 6 First half of chromosome with binary information

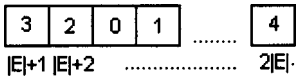

Fig. 7 Second half of chromosome with mating angle information

The optimal partitioning of G can be represented mathematically by a vector $\mathbf{x}=(x_i)$ where x_i is a binary variable representing the presence of edge e_i in the decomposition defined by the partitioning P. From the above, it is obvious that $i=1,\ldots,|E|$ since there are $|E|$ edges in the topology graph. Finally the problem is defined as:

Given G, the topology graph of the structure, F, set of mating features and k, number of substructures, find vector $\mathbf{x}$, partition representing the optimal decomposition, and vector $\mathbf{y}$, the mating feature for each joint subject to $f(\mathbf{x},\mathbf{y})$, which is an objective function to be minimized evaluating the decomposition quality.

3.4.2 Definition of the Constraints. The constraint on the vector $\mathbf{x}$, which represents the presence of edges, is as follows:

$$\text{COMPONENTS}(\text{GRAPH}(\mathbf{X}))=K \tag{2}$$

where

- GRAPH($\mathbf{x}$) returns a graph after the edges with $x_i=0$ in vector $\mathbf{x}$, have been removed from the original topology graph.
- COMPONENTS(G) returns the number of disconnected subgraphs in graph G.

This constraint translates into the fact that the problem asks for a decomposition consisting of k different structural members. The constraint on vector $\mathbf{y}$ is as follows:

$$y_i \in F \tag{3}$$

where F is the set of mating angles at which spot welds can be applied at the joints. One element of set F represents the case for no weld at the corresponding joint. The last constraint is imposed on the combination of the vectors x and y in the following way:

$$\text{CONNECTED}(\text{COMBINED\_GRAPH}(\mathbf{x},\mathbf{y}))=\text{TRUE} \tag{4}$$

where

- CONNECTED(G) returns TURE if the graph G is connected and returns FALSE otherwise.
- COMBINED_GRAPH($\mathbf{x}$,$\mathbf{y}$) returns a graph that consists of the nodes of the original graph and the edges in vectors $\mathbf{x}$ and $\mathbf{y}$.

This constraint ensures that the combination of the decomposition given by vector $\mathbf{x}$ and the mating angles given by vector $\mathbf{y}$ constitutes a structure which has the same connectivity as the original disconnected structure.

3.4.3 Definition of the Objective Function. Objective function will evaluate each decomposition according to the following criteria:

- Reduction of structural strength due to the introduction of joints
- Assembleability of the decomposed structure

To evaluate the decomposition according to the structural strength criteria, the normal stress at the joints and the area on which the normal stress acts are calculated using the Finite Element analysis of the original bitmap image *before* image processing (Fig. 3(*a*)). The evaluation is based on the difference between the angle, at which the normal stress is minimum, θ_i^{ideal}, and the chosen welding angle given by vector $\mathbf{y}$ because deviation from the ideal angle means higher normal stress. The stress at the chosen angle multiplied by the weld area provides a measure of force acting on the weld which is also used in evaluating the decrease in strength. A weld with larger area introduces a higher amount of decrease in strength than a weld with smaller area. Since the shape of the

original image does not change during decomposition process, the joint strength is estimated with the FEM result of the original image, without re-analyzing each potential decomposition. This approximation is adopted to ensure the real-time feedback to the designer, essential for tools during the conceptual design stage.

To evaluate the decomposition according to the assembleability criteria, the similarity of weld angles and the number of welds in the decomposition are taken into account. It should be noted that a structure decomposed into the same number of components can have different numbers of welds. For a given number of components, obviously, a lower number of welds and similar weld angles result in higher assembleability. These criteria result in the following objective function:

$$f(\mathbf{x},y)=w_1\sum_{i=1}^{N_{\text{welds}}}(\theta_i-\theta_i^{\text{ideal}})^2+w_2\sum_{i=1}^{N_{\text{welds}}}(\sigma_i(\theta_i)A_i(\theta_i))$$
$$+w_3\sum_{i=1}^{N_{\text{welds}}}\sum_{j=i+1}^{N_{\text{welds}}}(\theta_i-\theta_j)^2+w_4N_{\text{welds}} \quad (5)$$

The variables in the objective function are defined as follows:

- $\mathbf{x}=(x_i)$ x_i is a binary variable representing the presence of edge e_i in subset x
- $\mathbf{y}=(y_i)$ y_i is discrete variable representing the choice of weld angle at joint i
- w_i weight of ith criteria in the objective function
- N_{welds} total number of welds in the decomposed structure
- θ_i weld angle with respect to vertical direction at joint i
- θ_i^{ideal} angle of minimum normal stress at joint i
- $\sigma_i(\theta_i)$ normal stress at joint i at angle θ_i
- $A_i(\theta_i)$ weld area at joint i (function of θ_i)

The constraints and objective function combine to give the following optimization problem:

minimize $f(x,y)$ (as given in Eq. (5))

subject to

$$\text{COMPONENTS}(\text{GRAPH}(x))=k,$$

$$\text{CONNECTED}(\text{COMBINED\_GRAPH}(\mathbf{x},\mathbf{y}))=\text{TRUE}$$

$$x_i\in[0,1],\quad i=1,\ldots,|E|$$

$$y_i\in F,\quad i=1,\ldots,|E|$$

where F is the set of mating angles.

3.5 Optimization Method and Implementation

3.5.1 Genetic algorithm. Graph partitioning problem is NP-complete [23] even with simple linear criteria, which is to say that no polynomial-time algorithm is likely to exist. As a consequence all known algorithms that solve graph partitioning problems exactly have run-times exponential to the size of the graph. In this case the cost function is nonlinear and since we cannot afford exponential computation, heuristic algorithms are found to be suitable. More specifically, a genetic algorithm has been used to solve the problem approximately, *i.e.*, the algorithm may not give an optimal solution all the time.

The decomposition problem has been solved by using a steady-state genetic algorithm. Genetic algorithms [24,25] are a compromise between random and informed search methods, where variables are mapped to chromosomes and new generations are created by crossover (combining portions of two chromosomes) and mutation (randomly changing the values in each gene in a chromosome) until a termination condition is satisfied. In this project, the termination condition is satisfied when a given number of generations have evolved. A steady-state genetic algorithm [26] has been used and the following is the basic steps of steady-state GA:

1. Randomly create a population P of n chromosomes (an encoded representation of design variables) and evaluate their fitness values and store the chromosome with the *minimum* fitness value. Also create an empty subpopulation Q.
2. Select two chromosomes c_i and c_j in P with probability proportional to $(f_{\max}-f_i)$ and $(f_{\max}-f_j)$, respectively, where f_i and f_j are the fitness value of chromosome c_i and c_j, and $f_{\max}$ is the maximum fitness in P at the current generation.
3. Crossover c_i and c_j to generate two new chromosomes c_i' and c_j'.
4. Mutate c_i' and c_j' with a certain low probability.
5. Evaluate the fitness values of c_i' and c_j' and add them in Q. If Q contains less than m new chromosomes, go to 2.
6. Replace m chromosomes in P with the ones in Q and empty Q. Update the best chromosome and increment the generation counter. If the generation counter has reached a prespecified number, terminate the process and return the best chromosome. Otherwise go to 2.

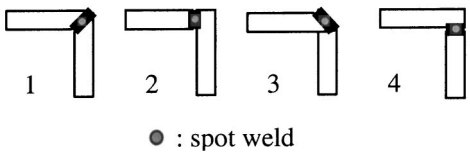

Fig. 8 Possible mating angles at the joints

It is assumed that the fitness is to be *minimized* in the above steps. Known empirical advantages of steady-state GA [26] are that SSGA prevents premature convergence of population and reaches an optimal solution with fewer number of fitness evaluations.

3.5.2 Chromosome representation of the problem. Each solution is encoded in a chromosome of the following nature. The chromosome is of length $2|E|$. First $|E|$ genes carry binary information about which edges of the topology graph are kept and which are removed to produce a decomposition. If the ith element of the chromosome is 0, it means that this edge has been cut in this particular decomposition represented by this chromosome. The second half of the chromosome carries the information about which discrete choice of possible mating angles is chosen for a given joint. The $(|E|+i\text{th})$ element carries the choice of mating angle for the ith joint (edge in the graph).

For this project, the possible mating angles have been chosen as 45, 0, 45, 90 degrees from the vertical and map to gene values of 1, 2, 3, 4, respectively, as illustrated in Fig. 8. A gene value of zero means no weld at that intersection. The possible weld angles are limited to 45 degree increment since the method is meant to be used during the conceptual design stage, when obtaining the ''optimal'' mating angle has less significance then simplicity, due to the uncertainly in the detailed component geometry.

Note that the information carried by the first two half of the chromosome maps to vector $\mathbf{x}$ and the second half maps to vector y in the mathematical model. It should also be noted that not every chromosome configuration will give a ''real'' cut. Leaving out of some edges will still keep the whole structure connected, therefore, every decomposition has to be checked whether it results in a graph with at least two disconnected components. Obviously, ideal case is k-disconnected components.

Since chromosomes representing the decompositions carry two different kinds of information (x_i is binary and $y_i\in F$) the cross-over and the mutation operators have been customized. The cross-over operator treats the first and second halves of the chromosome separately. It implements the cross-over in two steps in which the first halves of chromosomes are crossed with first halves, and second halves are crossed with second halves which is practically a multi-point cross-over operator. Figure 9 illustrates the cross-over of two chromosomes in the way described. The mutation

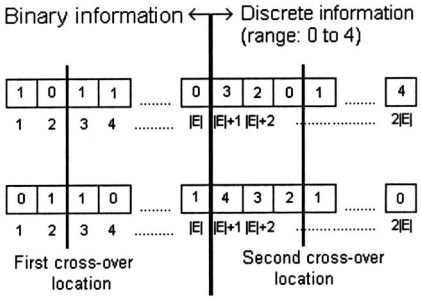

Fig. 9 Cross-over of two chromosomes.

operator is different from traditional mutation operators in that it increases the probability of mutation for the second half of the chromosome.

3.5.3 Fitness Evaluation of Chromosomes. Since genetic algorithms do not handle constraints directly, the constraints in the mathematical problem formulation have to be translated into penalty terms. Therefore, the fitness function will consist of two main terms which are the objective function value $f(\mathbf{x},\mathbf{y})$ of the decomposition and the penalty term which imposes the constraints of the mathematical model.

$$\text{fitness} = f(\mathbf{x},\mathbf{y}) + \text{penalty terms} \tag{6}$$

where objective function $f(\mathbf{x},\mathbf{y})$ is given as in Eq. (5). The mating angle from the vertical direction, θ_i, is calculated using the value in the $(|E|+i)$th gene in the following way:

$$\theta_i = (\text{gene}(|E|+i)-2)\times 45° \tag{7}$$

where gene $(|E|+i) \in F=\{0,1,2,3,4\}$ where 0 means no weld.

Ideal angle at the ith joint, θ_i^{ideal}, and stress tensors for each weld are obtained through an initial finite element analysis and stored in lookup tables. Normal stress at joint i at angle θ_i, $\sigma_i(\theta_i)$, is calculated using the stress tensor and the mating angle corresponding to the weld. A_i is the weld area calculated using the weld dimensions and the mating angle, i.e., it is a function of the mating angle, θ_i. Weld dimensions are calculated initially and stored in lookup tables.

Number of welds, N_{welds}, is the sum of edges for which the corresponding gene in the first half is zero and the gene in the second half is non-zero. Note that a zero in the first half means that the intersection has been cut and a non-zero value in the second half means that there is a weld.

The constraint on vectors **x** and **y** are imposed simply by the chromosome representation of the problem, i.e., genes in the first half of the chromosome are binary values imposing the constraint $x_i \in \{0,1\}$ and genes in the second half of the chromosome can only have values from 0 to 4 imposing the condition $y_i \in F$, where F is the set of possible mating angles. The constraint on the number of components (Eq. (2)) is imposed as a penalty in the fitness term:

$$\text{penalty} = w_s(\text{COMPONENTS}(\text{GRAPH}(\mathbf{x}))-k)^2 \tag{8}$$

The constraint to ensure the connectivity of the joined structure whole (Eq. (4)) is implemented by returning a fitness of infinity (very large number in the software implementation) for decompositions lacking connectivity, i.e., returning FALSE when passed to the CONNECTED function. Structurally disconnected decompositions, which are not feasible, are eliminated by this constraint implementation. The resulting fitness function (to be minimized) is as follows:

$$\text{fitness} = \begin{cases} \infty & \text{if CONNECTED(COMBINED\_GRAPH}(x,y)) \\ & \quad = \text{TRUE} \\ f(x,y) + w_5(\text{COMPONENTS}(\text{GRAPH}(x))-k)^2 & \\ \quad \text{otherwise} & \end{cases}$$

3.5.4 Software Implementation. The implementation has been done using the C++ programming language. For graph representation and related algorithms, the LEDA library developed at the Max-Planck Institute of Computer Science has been used. For GA implementation the GALib developed at the MIT CAD Lab was used. For the finite element analysis of the structure ABAQUS was used.

4 Examples

This section describes the topology extraction and decomposition of two example structures. The first example is a cantilevered structure in Fig. 2 subject a single load, and the second is a bridge-like structure subject to multiple point loads. In both examples, steel (Young's modulus 200 GPa; Poisson's ratio 0.3) is used as material. The input images are obtained by using the Topology optimization Web site at the Technical University of Denmark (http://www.topopt.dtu.dkl) and converting gray-scale information to binary information.

4.1 Cantilever Structure. The cantilever structure shown in Fig. 2 is decomposed to 3 and 4 components. The rectangular design domain of size 45 mm by 22 mm is fixed at the left edge and subject to downward load $P=10$ kN at the middle point of the right edge.

As shown in Fig. 10(f), all distinct ''members'' in the input image are successfully segmented as a result of the image transformation. Note since the original image in Fig. 10(a) is already smooth, dilation has little effect as evident from Fig. 10(b). The dilation algorithm has been applied using a 3×3 window and the Hough transform has been applied using 64 discretization levels for both dimensions of the θ-ρ space.

Figure 11(a) and (b) show the extracted product topology with the label for each member and the resulting product topology graph, respectively. On the topology graph, the intersections, which are candidates for joints are also labeled.

The next stage involves the application of the optimization method, namely GA, to the obtained product topology graph. This stage is preceded by a finite element analysis of the original bitmap image before image processing, where each pixel was treated as a finite element. Figure 12 shows the resulting von Mises stress plot, where gray scale table on the left ranges from 183 Pa (light) to 12.3 k Pa (dark). The results of the finite element analysis are stored in a look-up table to be used during chromosome evaluation. The following GA parameters were used:

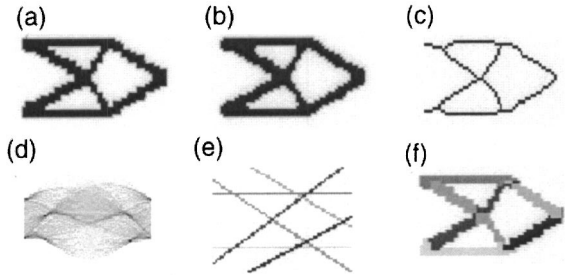

Fig. 10 Result of topology extraction (*a*) original image, (*b*) dilation, (*c*) skeletonization, (*d*) initial Hough transform (shown in θ-ρ space), (*e*) primary line extraction, and (*f*) topological segmentation

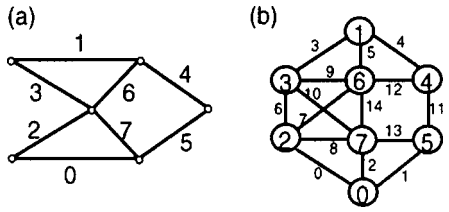

Fig. 11 Construction of the product topology graph: (*a*) extracted product topology and (*b*) the resulting product topology graph

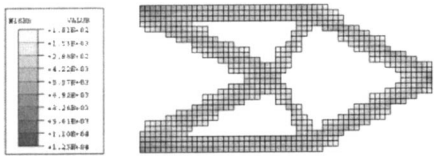

Fig. 12 von Mises stress plot of the original bitmap image. The gray scale table on the left ranges from 183 MPa (light) to 12.3 GPa (dark). Maximum stress in the structure is approximately 500 MPa.

- Population size = 200
- Number of generations = 1000
- Replacement percentage = 30%
- Crossover probability = 0.9
- Mutation probability = 0.1 (double for second half of chromosome since it carries non-binary information)

Since the fitness evaluations do not involve finite element analyses, the computation takes, for example, less than one minute even with a 200 MHz Pentium laptop computer with a 32 MB RAM.

The solution for the case when three components were specified is represented by the chromosome shown in Table 1. Figure 13 illustrates the decomposition of the product topology graph that this chromosome maps to and the corresponding product decomposition. It is observed that the resulting decomposition is *not* symmetric, while the original structure is symmetric. Since no symmetricity is imposed in the problem formulation, the algorithm simply chose the decomposition as low fitness value as possible, which happened to be asymmetric (see Fig. 15 for comparison) for this 3-component decomposition. In fact, a seemingly "natural" symmetric decomposition consisting of three members {1, 3, 6}, {2, 0, 7} and {4, 5} gives higher objective function value (i.e., is a worse decomposition) for this particular run. The dashed lines in the graph represent the edges that have been cut during the decomposition and have been selected as the welding points. It is noteworthy that only some of the edges in the graph, which have been cut, have been selected as welding locations as a result of the objective to minimize number of welds. However, the connectivity of the initial structure is still preserved.

Table 1 Resulting chromosome for 3-component decomposition.

Edge no	0	1	2	3	4	5	6	7	8	9	10	11	12	13	14
1st half of chromosome	1	1	1	1	0	1	0	0	1	1	0	0	0	1	0
2nd half of chromosome	4	1	4	1	0	4	0	0	0	4	0	3	3	3	3

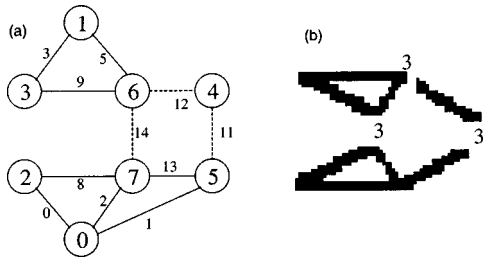

Fig. 13 Resulting decomposition of (*a*) the product topology graph, and (*b*) the structure decomposed into 3 components

Table 2 Joint angles in the 3-component decomposition

Edge no.	Joint angle	θ^{ideal}
11	45°	37.263°
12	45°	22.880°
14	45°	44.525°

The results obtained satisfy the defined criteria for a good decomposition. Desired number of components of decomposed structure has been achieved, i.e., the decomposition has three components. For three components, a decomposition with three welds has been found where three is the minimum number of welds needed to preserve connectivity. The objective to have similar weld angles has also been achieved. Table 2 shows a summary of the obtained and ideal joint angles. All welds are chosen to be at angle three (45 deg). These results intuitively make sense since 45 deg is the maximum shear angle for cantilever beam subject to pure bending, indicated by the closeness to θ^{ideal} shown in the third column of Table 2. A close examination of the optimization results indicates all joints are in fact are under compression and shear. Figure 14 shows the typical optimization history. Major improvements in the fitness value are achieved during the first 150 generations.

The solution that the optimization algorithm found when four components were specified was represented by the chromosome shown in Table 3. Figure 15 illustrates the decomposition of the product topology graph into four components that this chromosome maps to and the corresponding product decomposition. In this case, the resulting decomposition is symmetric, adding one joint at edge 13 to the 3-component decomposition in Fig. 13. Table 4 shows a summary of the obtained and ideal joint angles. Again, all welds are under compression and shear. The minimum number of welds needed to preserve connectivity has been achieved which is four. The objective to have similar weld angles has also been achieved, i.e., all welds are at angle three which maps to 45 deg from the vertical direction.

4.2 Bridge-like Structure. As a second example, the bridge-line structure shown in Fig. 16 is decomposed to 4 and 6 components. The rectangular design domain of size 44 mm by 22 mm is simply supported at the lower left corner and fixed at the lower right corner, and subject to three downward loads of 3 kN at the location shown in Fig. 16. Figure 17 show the topology extraction process of this structure. The window size for the dilation

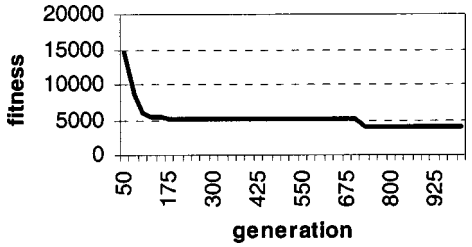

Fig. 14 Optimization history of 3 component decomposition of the cantilever

Table 3 Resulting chromosome for 4-component decomposition

Edge no	0	1	2	3	4	5	6	7	8	9	10	11	12	13	14
1st half of chromosome	1	0	1	1	0	1	0	0	1	1	0	0	0	0	0
2nd half of chromosome	3	0	3	3	0	3	0	0	3	4	0	3	3	3	3

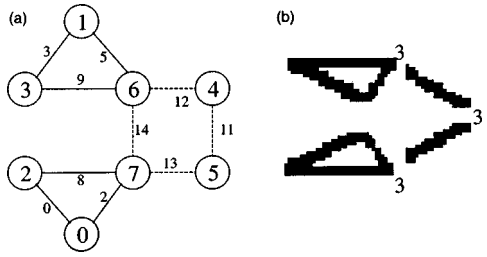

Fig. 15 Resulting decomposition of (*a*) the product topology graph, and (*b*) the structure decomposed into 4 components

algorithm is 3 by 3 and the θ-ρ space for Hough transform is discretized to 128 by 128. In Fig. 17(a), the middle two segments in the structure became slightly wider than the left one after the binarization of the grayscale image in Fig. 16 (obtained as a GIF image at http://www.topopt.dtu.dk/), due to a numerical error.

The segmentation of the image results in the product topology graph shown in Fig. 18. While the input structure is symmetric, the product topology graph in Fig. 18(*b*) is asymmetric. This is because member 3 was not segmented adjacent to member 11 in Fig. 17(*e*) due to the noise in the original binary image (Fig. 17(*a*)). Figure 19 shows the von Mises stress plot of the finite element analyses of this bitmap image.

The parameters for GA are the same as the first example, except that the population size is increased to 400. The result of a 4-component decomposition is given in Fig. 20. The decomposition is asymmetric. Table 5 shows some deviation from the ideal joint angle and the obtained joint angles in edge 13 and 17. A close examination of the optimization results indicate this was due to the effect of the second term in the objective function (Eq. (5)), which tries to minimize the force acting on the prospective joints.

Figure 21 and Table 6 show the result of the same structure decomposed to 6 components. Although the joint locations are not completely symmetric (Fig. 21(*a*)), the corresponding components are symmetric (Fig. 21(*b*)). Similar to the case of 4-component decomposition, deviations from ideal angles are exhibited at joints in Table 6, which are subject to relatively a large force.

Table 4 Joint angles in the 4-component decomposition

Edge no.	Joint angle	θ^{ideal}
11	45°	37.263°
12	45°	22.880°
13	45°	15.289°
14	45°	44.525°

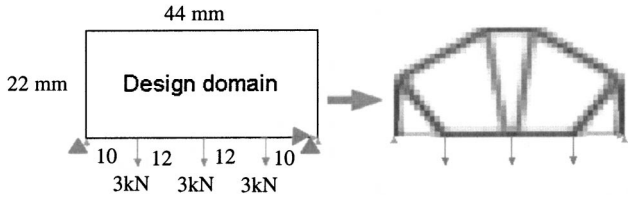

Fig. 16 Structural topology design of a bridge-like structure for maximum stiffness occupying 30% of the design domain

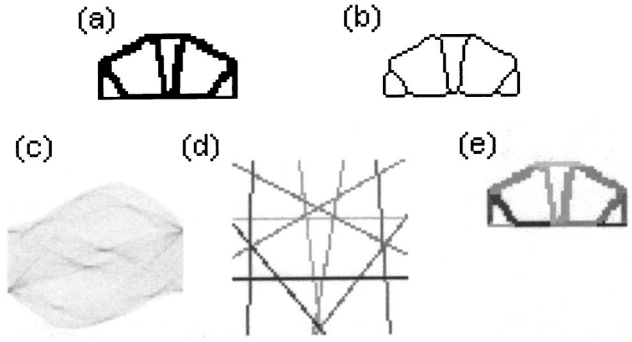

Fig. 17 Result of topology extraction (*a*) original image, (*b*) dilation, (*c*) skeletonization, (*d*) initial Hough transform (shown in θ-ρ space), (*e*) primary line extraction, and (*f*) topological segmentation

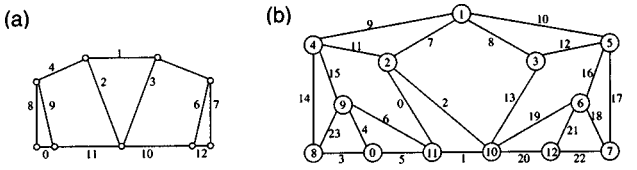

Fig. 18 Construction of the product topology graph: (*a*) extracted product topology and (*b*) the resulting product topology graph

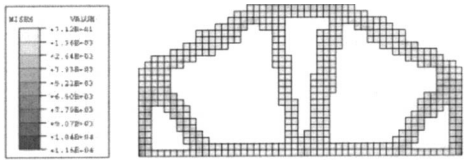

Fig. 19 von Mises stress plot of the original bitmap image. The gray scale table on the left ranges from 71 MPa (light) to 11.6 GPa (dark). Maximum stress in the structure is approximately 500 MPa.

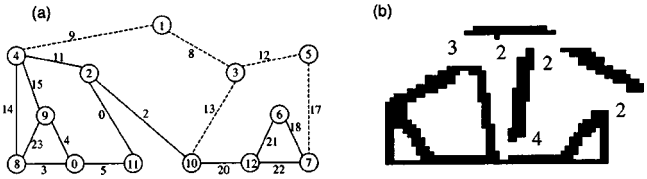

Fig. 20 Resulting decomposition of (*a*) the product topology graph, and (*b*) the structure decomposed into 4 components

Table 5 Joint angles in the 4-component decomposition

Edge no.	Joint angle	θ^{ideal}
8	0°	-6.459°
9	45°	31.502°
12	0°	-7.293°
13	90°	-9.683°
17	0°	-33.357°

5 Discussion and Future Work

The presented method seems capable of quickly evaluating candidate decompositions according to the defined criteria. The results in the examples satisfy the defined criteria for a good decomposition. Desired number of components of decomposed structure

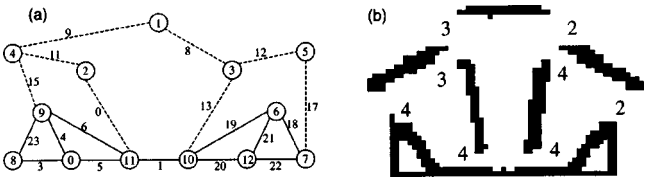

Fig. 21 Resulting decomposition of (*a*) the product topology graph, and (*b*) the structure decomposed into 6 components

Table 6 Joint angles in the 6-component decomposition

Edge no.	Joint angle	θ^{ideal}
0	90°	-4.153°
8	0°	-6.459°
9	45°	31.502°
11	45°	8.244°
12	0°	-7.293°
13	90°	-9.683°
15	90°	30.986°
17	0°	-33.357°

has been achieved in both results. Chosen weld angles eliminate tensile stress on welds, i.e., all welds are under compression. The number of welds has been minimized in all solutions. The objective to have similar weld angles has also been achieved. In both solutions all welds are at the same angle.

In the examples, the weight for each criterion is determined through many trials. It is observed that the results of decomposition vary depending on the weights. Since different weight can yield a different high-performance, if not Pareto-optimal, decomposition, it is expected the method can be an effective exploration tool during the conceptual design stage.

The future work includes the adoption of more decomposition criteria such as the distance between welding spots, the accessibility of welding spots, the ease of fixturing during assembly, and the ease of component manufacturing. Also, more detailed modeling of joint features can be done to achieve more accurate evaluation of the effect of joints on overall structural strength. Finally, the extension to 3-D structures is necessary for the demonstration of the effective in practical examples.

Acknowledgments

This work was supported by the National Science Foundation under CAREER Award (DMI-9984606), Toyota Motor Corporation, and the Horace H. Rackham School of Graduate Studies at the University of Michigan. These sources of support are gratefully acknowledged. The authors acknowledge Mr. Onur Cetin for his help during the revision of the manuscript.

References

[1] Boothroyd, G., and Dewhurst, P., 1983, *Design for Assembly Handbook*, University of Massachusetts, Amherst.
[2] Bourjault, A., 1984, ''Contribution a une Approche Méthodoligique de L'Assemblage Automatisé: Elaboration Automatique des Séquences Opératoires,'' Ph.D. Thesis, Université de Franche-Comté, Besançon, France.
[3] de Fazio, T., and Whitney, D., 1987, ''Simplified Generation of All Mechanical Assembly Sequences,'' IEEE J. Rob. Autom., **RA-3**(6), pp. 640–658. Corrections on same journal, **RA-4**(6); pp. 705–708.
[4] de Mello, L. Hommem, and Sanderson, A., 1991, ''A Correct and Complete Algorithm for the Generation of Mechanical Assembly Sequences,'' IEEE Trans. Rob. Autom., **7**(2), pp. 228–240.
[5] Lee, S., and Shin, Y., 1990, ''Assembly Planning Based on Geometric Reasoning,'' Comput. Graph., **14**(2), pp. 237–250.
[6] de Fazio, T., Edsall, A., Gustavson, R., Hernandez, J., Hutchins, P., Leung, H.-W., Luby, S., Metzinger, R., Nevins, J., Tung, T., and Whiteney, D., 1993, ''A Prototype of Feature-based Design for Assembly,'' ASME J. Mech. Des., **115**, pp. 723–734.
[7] Lee, S., Kim, G., and Bekey, G., 1993, ''Combining Assembly Planning with Redesign: An Approach for More Effective DFA,'' *Proceedings of 1993 IEEE International Conference on Robotics and Automation*, pp. 319–325.
[8] Hsu, W., Lee, C., and Su, S., 1993, ''Feedback Approach to Design for Assembly by Evaluation of Assembly Plan,'' Comput.-Aided Des., **25**(7), pp. 395–410.
[9] Mantripragada, R., Cunningham T., and Whitney, D., 1996, ''Assembly Oriented Design: A New Approach to Designing Assemblies,'' *Proceedings of IFIP Workshop on Geometric Modeling and CAD*, pp. 308–324, Airlie, VA.
[10] Mantripragada, R., 1998, ''Assembly Oriented Design: Concepts, Algorithms and Computational Tools,'' PhD Thesis, Massachusetts Institute of Technology, Cambridge.
[11] Bosák, J., 1990, *Decompositions of Graphs*, Kluwer Academic Publications, Boston.
[12] Michelena, N., and Papalambros, P., 1995, ''Optimal Model-based Decomposition of Powertrain System Design,'' ASME J. Mech. Des., **117**(4), pp. 499–505.
[13] Rosen, D., Dixon, J., and Finger, S., 1994, ''Conversions of Feature-based Design Representations Using Graph Grammar Parsing,'' ASME J. Mech. Des., **116**, pp. 785–792.
[14] Wang, C.-H., and Bourne, D., 1997, ''Concurrent Decomposition for Sheet-metal Products,'' *Proceedings of 1997 ASME Design Engineering Technical Conference*, Sacramento, CA.
[15] Wang, C.-H., 1997, ''Manufacturability-Driven Decomposition of Sheet Metal Products,'' PhD thesis, Carnegie Mellon University.
[16] Saitou, K., and Yetis, F. A., 2000, ''Decomposition-Based Assembly Synthesis of Structural products: Preliminary Results,'' *Proceedings of the Third International Symposium on Tools and Methods of Competitive Engineering* Delft, The Netherlands, April 18–21, pp. 477–486.
[17] Yetis, F. A., and Saitou, K., 2000, ''Decomposition-based Assembly Synthesis Based on Structural Considerations,'' *Proceedings of the 2000 ASME Design Engineering Technical Conferences*, Baltimore, Maryland, September 10–13, DETC2000/DAC-1428.
[18] Yetis, F. A., 2000, ''Decomposition-Based Assembly Synthesis of Structural Products,'' Master's thesis, University of Michigan.
[19] Bendsøe, M. P., and Kikuchi, N., 1988, ''Generating Optimal Topologies in Structural Design Using a Homogenization Method,'' Comput. Methods Appl. Mech. Eng., **71**, pp. 197–24.
[20] Chapman, C. D., Saitou, K., and Jakiela, M. J., 1994, ''Genetic Algorithms as an Approach to Configuration and Topology Design,'' ASME J. Mech. Des., **116**, pp. 1005–1012.
[21] Gonzalez, R. C., and Wintz, P., 1987, *Digital Image Processing*, Addison Wesley, Reading, Massachusetts, second edition.
[22] Ballard, D. H., 1981, ''Generalizing the Hough Transform to Detect Arbitrary Shapes,'' Pattern Recogn., **13**(2), pp. 111–122.
[23] Garey, M. R., and Johnson, D. S., 1979, *Computers and Intractability, a guide to the theory of NP-completeness*, W. H. Freeman and Company, New York.
[24] Goldberg, D., 1989, *Genetic Algorithms in Search, Optimization, and Machine Learning*, Addison-Wesley, Reading, Massachusetts.
[25] Holland, J., 1975, *Adaptation in Natural and Artificial Systems*, The University of Michigan Press, Ann Arbor, Michigan.
[26] David, L., 1991, *Handbook of Genetic Algorithms*, Van Nostrand Reinhold, New York.